Electronic Supplementary Material (ESI) for CrystEngComm.
This journal is © The Royal Society of Chemistry 2015

4-Aminoquinaldine monohydrate polymorphism: Prediction and impurity aided discovery of a difficult to access stable form

Doris E. Braun, Herbert Oberacher, Kathrin Arnhard, Maria Orlova and Ulrich J. Griesser

Electronic Supplementary Information

Contents of Supplementary Information

1 COMPUTATIONAL

1.1 Space groups

Z'=1 monohydrate structures were randomly generated in following 48 space groups, $P1$, $P\bar{1}$, $P2_1$, $P2_1/c$, $P2_12_12$, $P2_12_12_1$, $Pna2_1$, $Pca2_1$, $Pbca$, $Pbcn$, $C2/c$, Cc, $C2$, Pc, Cm, $P2_1/m$, $C2/m$, $P2/c$, $C222_1$, $Pmn2_1$, $Fdd2$, $Pnna$, $Pccn$, $Pbcm$, $Pnnm$, $Pmmn$, $Pnma$, $P4_1$, $P4_3$, $I\bar{4}$, $P4/n$, $P4_2/n$, $I4/m$, $I41/a$, $P41212$, $P4_32_12$, $P3_1$, $P3_2$, $R3$, $P\bar{3}$, $R\bar{3}$, $P3_121$, $P322_1$, $R3c$, $R\bar{3}c$, $P6_1$, $P6_3$, $P6_3/m$.

1.2 DFT-D Calculations: Methodology

The DFT-D calculations were carried out with the CASTEP plane wave code[1] using the Perdew-Burke-Ernzerhof (PBE) generalised gradient approximation (GGA) exchange-correlation density functional[2] and ultrasoft pseudopotentials,[3] with the addition of a semi-empirical dispersion correction, either the Tkatchenko and Scheffler (TS) model,[4] or Grimme06 (G06).[5] In a first step, the structures were geometry optimised using the TS dispersion correction. Brillouin zone integrations were performed on a symmetrised Monkhorst–Pack *k*-point grid with the number of *k*-points chosen to provide a maximum spacing of 0.07 $Å^{-1}$ and a basis set cut-off of 560 eV. The self-consistent field convergence on total energy was set to $1x10^{-5}$ eV. Energy minimisations were performed using the Broyden–Fletcher–Goldfarb–Shanno optimisation scheme within the space group constraints. The optimisations were considered complete when energies were converged to better than $2x10^{-5}$ eV per atom, atomic displacements converged to $1x10^{-3}$ Å, maximum forces to $5x10^{-2}$ eV $Å^{-1}$, and maximum stresses were converged to $1x10^{-1}$ GPa. Energy minimisations with variable unit cells were restarted after the first minimisation to reduce the effects of changes in unit cell on the basis set. The energies for the monohydrates were recalculated, without optimisation, with the number of *k*-points chosen to provide a maximum spacing of 0.04 $Å^{-1}$ and a basis set cut-off of 780 eV, using the G06 dispersion correction, resulting in the final crystal energy landscape (Fig. 3). Isolated molecule minimisations to compute the isolated **4-AQ** and water energy (U_{gas}) were performed by placing a single molecule in a fixed cubic 35x35x35 $Å^3$ unit cell and optimised and recalculated with the same settings used for the crystal calculations.

1.3 Lowest Energy Structures (CrystalOptimizer and PBE-G06)

All calculated structures are available in .res format from the authors on request. The lowest energy structures derived from CryOpt and DFT-D calculations are given in Tables S1 and S2, respectively.

Table S1. Hypothetical and known low-energy crystal structures (CryOpt).

Str. ID[a]	Space group	Cell parameters						E_{latt}/ kJ mol^{-1}	ΔE_{latt}/ kJ mol^{-1}	Density g cm^{-3}
		a/Å	b/Å	c/Å	α/°	β/°	γ/°			
548 (Hy1$_B$°)	$P2_1/c$	4.525	12.85	15.65	90	99.34	90	–176.66	0	1.303
1 (Hy1$_A$)	$Pna2_1$	4.736	13.636	14.269	90	90	90	–172.65	4.01	1.270
10	$Pna2_1$	4.737	13.541	14.300	90	90	90	–169.89	6.77	1.276
315	$Pna2_1$	9.239	6.752	14.875	90	90	90	–167.78	8.88	1.261
11	$P2_1/c$	4.732	14.994	13.607	90	74.31	90	–166.71	9.95	1.259
81	$P2_1/c$	4.692	15.056	13.520	90	78.82	90	–166.27	10.39	1.249
7	$P2_12_12_1$	16.597	4.712	11.737	90	90	90	–166.26	10.40	1.275
30	$Pna2_1$	4.806	12.505	16.072	90	90	90	–165.17	11.49	1.212
86	Cc	4.727	15.178	13.082	90	81.86	90	–164.46	12.20	1.260
408	$P2_1/c$	9.364	12.920	8.588	90	65.26	90	–164.13	12.53	1.241
19	Cc	13.063	14.991	4.778	90	81.74	90	–163.96	12.70	1.264
192	$Pna2_1$	4.766	12.434	16.408	90	90	90	–163.96	12.70	1.204
48	Cc	14.693	13.762	4.819	90	94.00	90	–163.73	12.93	1.204
225	$Pna2_1$	4.851	13.231	14.546	90	90	90	–163.13	13.53	1.254
1772	$P2_1/c$	8.461	15.550	7.834	90	65.52	90	–161.85	14.81	1.248
1593	$P2_1/c$	4.377	18.783	11.859	90	95.77	90	–161.87	14.79	1.274
1184	$Pna2_1$	9.111	6.999	14.823	90	90	90	–161.55	15.11	1.238
1280	$P2_1/c$	8.771	14.553	8.131	90	112.89	90	–161.35	15.31	1.224
1447	Pc	7.902	4.457	14.243	90	105.66	90	–161.15	15.51	1.212
84	$P2_1/c$	11.995	8.635	9.122	90	77.59	90	–160.98	15.68	1.269
740	$P2_1/c$	8.978	8.630	12.135	90	81.74	90	–160.81	15.85	1.258
149	$P2_1/c$	7.652	15.529	7.890	90	75.44	90	–160.79	15.87	1.290
1343	Cc	4.771	13.924	15.145	90	76.05	90	–160.56	16.10	1.199
707	$C2/c$	13.165	9.100	15.625	90	85.86	90	–160.32	16.34	1.254
430	$C2/c$	15.372	9.124	14.180	90	107.66	90	–160.19	16.47	1.235
51	$P2_1/c$	7.135	17.569	7.207	90	92.80	90	–159.81	16.85	1.300
135	$P2_1/c$	3.847	15.990	16.879	90	78.80	90	–159.69	16.97	1.270
722	$Pna2_1$	14.391	14.375	4.581	90	90	90	–159.53	17.13	1.235
100	$Pna2_1$	11.784	17.025	4.613	90	90	90	–159.53	17.13	1.265
59	$P2_1/c$	11.862	8.719	9.030	90	80.33	90	–159.45	17.21	1.271
514	$P2_1/c$	7.078	7.726	17.210	90	76.80	90	–159.22	17.44	1.277
1755	$P\bar{1}$	9.322	8.707	9.883	101.87	58.55	62.15	–159.06	17.60	1.204
389	Cc	8.755	16.330	8.319	90	126.85	90	–159.02	17.64	1.230
294	$P2_12_12_1$	16.776	13.625	3.920	90	90	90	–158.79	17.87	1.306
233	Pc	4.250	9.184	12.294	90	95.89	90	–158.29	18.37	1.226

[a]Structure ID corresponds to the CrystalPredictor ranking.

Table S2. Hypothetical and known low-energy crystal structures (PBE-G06), Fig. 3.

Str. ID[a]	exp.	Space group	Cell parameters						E_{latt}/ kJ mol^{-1}	ΔE_{latt}/ kJ mol^{-1}	PI[b]/ %	Void Space[c]
			a/Å	b/Å	c/Å	α/°	β/°	γ/°				
1_548	Hy1$_B$°	$P2_1/c$	4.483	12.284	16.001	90	94.09	90	–212.86	1.332	74.8	0.0
2_1	Hy1$_A$	$Pna2_1$	4.537	13.798	14.296	90	90	90	–212.13	1.308	73.3	0.0
3_10		$Pna2_1$	4.595	13.714	14.174	90	90	90	–210.89	1.310	73.3	0.0
4_86		Cc	12.852	15.343	4.546	90	97.34	90	–206.70	1.316	74.0	0.0
5_81		$P2_1/c$	4.542	15.191	13.261	90	97.39	90	–203.55	1.290	72.4	0.0
6_30		$Pna2_1$	4.632	12.365	16.230	90	90	90	–202.93	1.259	70.8	3.7
7_7		$P2_12_12_1$	4.712	11.491	16.612	90	90	90	–201.90	1.301	73.1	1.6
8_315		$Pna2_1$	8.929	6.742	15.101	90	90	90	–201.29	1.288	72.7	0.0
9_11		$P2_1/c$	4.681	15.112	12.894	90	93.64	90	–200.42	1.286	72.4	0.0

[a]Structure ID: rank PBE-G06_rank CrystalPredictor. [b]PI - Kitaigorodskii type of packing index, calculated using PLATON.[6] [c]Void space was calculated using a 1.0 Å probe radius and an approx. grid spacing of 0.1 Å and is given as % of unit cell volume.

1.4 Representation of the Experimental Structures

The computational models were successful in reproducing the experimental structures (Table S3). The computationally generated low energy structures were compared using the Solid Form module of Mercury to determine the root mean square deviation of the non-hydrogen atoms in a cluster of 15 molecules (rmsd$_{15}$).[7]

Table S3. Quality of representation of the CryOpt (CrystalOptimizer) and PBE-TS monohydrate structures.

	Lattice parameters (cell vectors/Å, angles/°)						cell volume (Å^3)	rmsd$_{15}$ (Å)
	a	*b*	*c*	*α*	*β*	*γ*		
Exptl., **Hy1$_A$**, LOBSOL, $Pna2_1$, RT	4.743	13.907	14.513	90	90	90	957.51	–
Calc., CryOpt, $Pna2_1$, 0K	4.736	13.636	14.269	90	90	90	921.58	0.17
Calc., PBE-TS, $Pna2_1$, 0K	4.537	13.798	14.296	90	90	90	894.94	0.17
Exptl., **Hy1$_B$**, $P2_1/c$, RT	4.783	12.077	16.337	90	92.23	90	943.07	–
Calc., CryOpt, $P2_1/c$, 0K	4.525	12.852	15.656	90	99.34	90	898.40	0.29
Calc., PBE-TS, $P2_1/c$, 0K	4.483	12.284	16.001	90	94.09	90	872.07	0.24

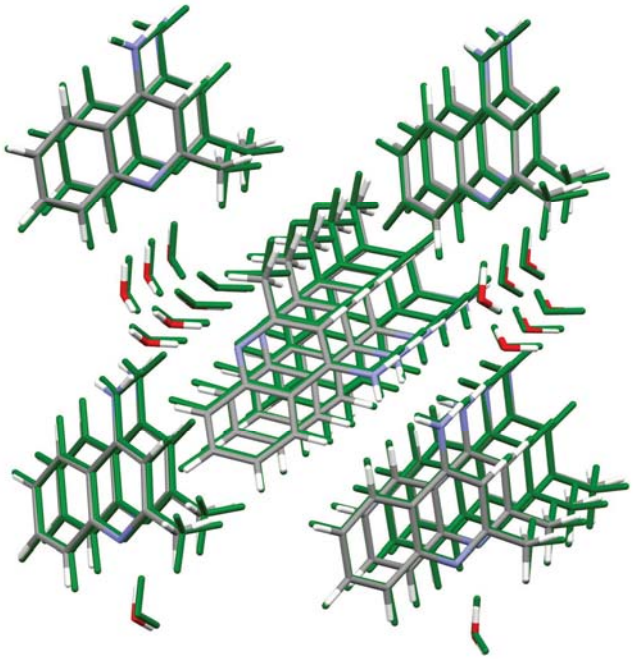

Figure S1. Overlay of the 30 molecule cluster of the observed structure of **Hy1$_A$** (coloured by element) and calculated PBE-TS structure (green), rmsd$_{15}$=0.17 Å.

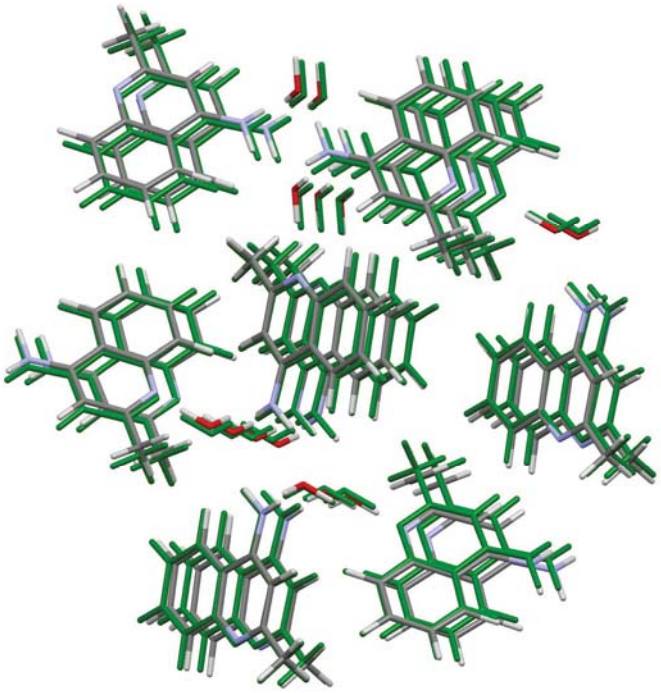

Figure S2. Overlay of the 30 molecule cluster of the observed structure of **Hy1$_A$** (coloured by element) and calculated PBE-TS structure (green), rmsd$_{15}$=0.24 Å.

1.5 PIXEL Calculations

PIXEL energies are intermolecular energies (i.e. U_{inter}) derived by integration over the isolated molecule charge densities placed in the crystal structures. The electrostatic contribution E_C is rigorously derived by this procedure and various approximations are used to estimate the polarisation (induction) E_P, dispersion E_D, and repulsion E_R contribution to the intermolecular lattice energy. The calculations also provide an approximate breakdown into contributions from different pairs of molecules in the coordination shell.

Table S4. PIXEL calculations on **4-AQ** lowest energy structures (**Hy1$_B$°**, **Hy1$_A$**, **3** - **6**). Only the most relevant intermolecular interactions for pairs of molecules are listed.

Structure	Interaction[a]	E_C[b]	E_P[c]	E_D[d]	E_R[e]	U_{inter}[f]
		kJ mol^{-1}				
Hy1$_B$° (1)	N–H1···O	–36.0	–11.5	–10.1	30.1	–27.4
*Pna*2$_1$	N–H2···O	–43.9	–16.5	–12.4	48.9	–24.0
	π···π	–5.6	–5.7	–41.8	30.3	–22.9
	O–H···N1	–87.6	–52.6	–21.4	138.9	–22.6
	O–H···N2	–36.6	–18.5	–11.9	49.0	–18.0
	short contacts	–7.2	–1.8	–11.9	5.1	–15.9
Hy1$_A$ (2)	N–H2···O	–87.6	–49.7	–22.8	133.2	–27.0
*P*2$_1$/*c*	N–H1···O	–41.9	–14.4	–9.3	40.9	–24.7
	C–H···π	–16.9	–9.3	–27.7	31.2	–22.7
	π···π	–2.7	–5.8	–43.0	31.6	–19.9
	O–H···O	–59.3	–25.4	–8.6	77.0	–16.4
3	O–H···N1	–85.9	–51.7	–21.9	135.1	–24.4
*Pna*2$_1$	C–H···π	–19.2	–10.1	–27.0	32.3	23.9
	π···π	–1.9	–5.4	–40.5	27.2	–20.6
	N–H1···O	–35.9	–14.5	–10.2	42.4	–18.2
	O–H···O	–61.2	–29.3	–9.3	84.3	–15.6
4	O–H···N1	–81.0	–44.9	–20.6	120.3	–26.1
Cc	N–H2···N2	–15.5	–8.5	–27.5	29.9	–21.6
	π···π	–5.0	–5.8	–40.7	31.3	–20.3
	short contacts	–8.9	–2.7	–20.3	13.6	–18.2
	N–H1···O	–31.0	–12.1	–9.6	34.8	–18.0
	O–H···O	–60.0	–27.0	–9.0	78.3	–17.7
5	N–H2···O	–38.0	–12.7	–13.4	36.4	–27.7
*P*2$_1$/*c*	O–H···N1	–84.2	–48.0	–21.4	127.8	–25.9
	N–H1···O	–39.6	–13.7	–9.8	38.0	–25.0
	π···π	–4.6	–5.5	–38.7	28.3	–20.6
	O–H···N2	–32.5	–16.8	–11.2	43.5	–17.0
	short contacts	–7.7	–2.0	–15.0	8.7	–16.0
6	O–H···N1	–65.5	–34.7	–18.9	87.9	–31.3
*Pna*2$_1$	O–H···O	–47.8	–18.8	–7.4	52.2	–21.9
	π···π	–6.1	–5.4	–42.9	33.8	–20.5
	N–H2···O	–25.1	–8.2	–8.2	21.1	–20.3
	N–H1···N2	–34.8	–18.6	–27.4	60.8	–20.0

[a]PIXEL energies are for a pair of molecules. The pairs of molecules are defined by the intermolecular interaction; [b]electrostatic (Coulombic) energy; [c]polarisation energy; [d]dispersion energy; [e]repulsion energy; [f]total intermolecular energy: $U_{inter} = E_C + E_P + E_D + E_R$. The non-additivity of E_P is not included.

It has to be noted that the non-additivity of the molecule···molecule polarisation energies could not be taken into account for calculating the dimeric energies given in Table S4. This error was estimated by considering the lattice energies obtained by summing the molecule-molecule pairwise energies. These energies differ from the PIXEL lattice energies when the polarisation is calculated from the net field (i.e. accounting for non-additivity of the electrostatic field around a molecule) by approximately a max. ± 3.6% error in U_{inter}. Thus the neglect of non-additivity and distant interactions does not qualitatively affect the results in the m/s.

1.6 Void Analysis

The Mercury Hydrate Analyzer tool was used to visualise the water/void space in the computed lowest energy structures. A probe radius of 1.0 Å and approximate grid spacing of 0.1 was applied to visualise the void space (Figure S3). Structures **Hy1$_B$°**, 5, 7, 8 and 9 have the water molecules at isolated sites whereas in structures **Hy1$_A$**, 3, 4 and 6 the water molecules form channels. Albeit, the water molecules form strong hydrogen bonds in the "channel" structures and may not be expected to show a non-stoichiometric (de)hydration behavior.

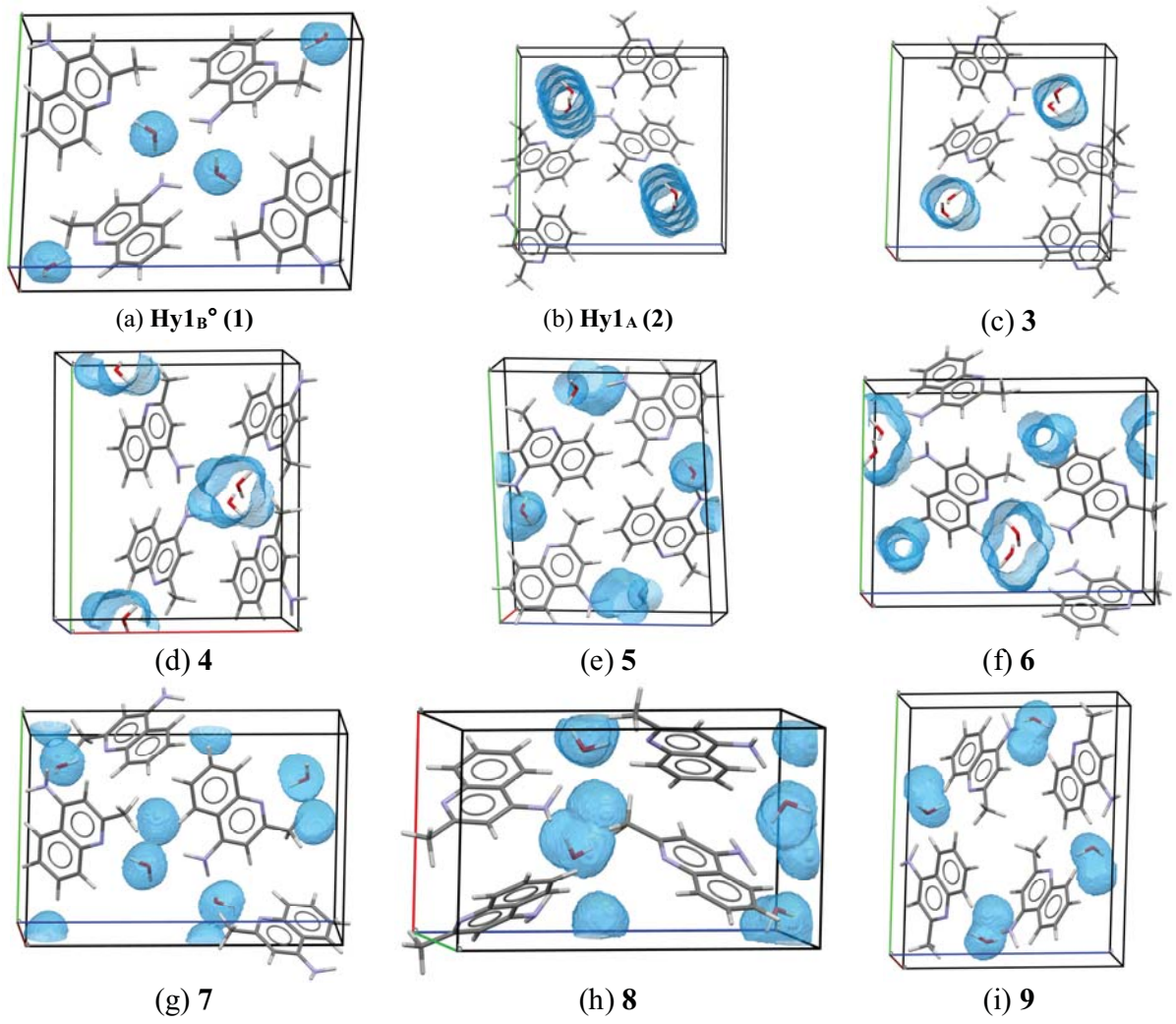

Figure S3. Solvent accessible voids containing waters of crystallisation in computationally generated low energy structures, calculated using a 1.0 Å probe radius.

2 EXPERIMENTAL

2.1 Impurity Profile of Commercial 4-AQ Samples

2.1.1 Optical Appearance

Figure S4. **4-AQ** (powder) as obtained from the supplier. Left: Sigma Aldrich (*SA*), right: Fluka (*F*).

2.1.2 Electrospray Ionization(ESI)-MS

ESI-MS was performed on a QSTAR XL mass spectrometer (AB Sciex, Framingham, MA, USA) equipped with a modified TurboIonSpray source (MicroTurboIonSpray). Modifications included the replacement of the Peek tubing transfer line and of the stainless steel sprayer capillary by fused silica capillaries (transfer line: 375 µm o.d., 20 µm i.d., sprayer capillary: 90 µm o.d., 20 µm i.d., Polymicro Technologies, Phoenix, AZ, USA). Mass calibration and optimisation of instrumental parameters were performed in the positive ion mode by infusion of a mixture of 1.0 mg/l caffeine and 1.0 mg/l reserpine dissolved in 0.05% aqueous formic acid solution containing 50% acetonitrile (v/v) at a flow rate of 2.0 µl/min. The spray voltage was 5.3 kV. Gas flows of 3 arbitrary units (nebulizer gas) and 30 arbitrary units (turbo gas) were employed. The temperature of the turbo gas was adjusted to 200 °C. To acquire MS and MS/MS spectra of 4-AQ and its impurities, solutions of 1.0 µg/ml *SA* and *F* in 0.05% aqueous formic acid containing 50% acetonitrile (v/v) were prepared and directly infused into the mass spectrometer at a flow rate of 2.0 µl/min. Mass spectra were collected in the range between 50 u and 700 u. For MS/MS, Q1 resolution was set to unit resolution. The collision gas (N_2) flow was set to 5 arbitrary units. Collision energies of 35 eV were applied to generate product ion mass spectra. The accumulation time was set to 1.0 sec. Spectra were collected from *m/z* 50 to *m/z* 700, and recorded on a personal computer with the Analyst QS software (1.0, service pack 8, AB Sciex).

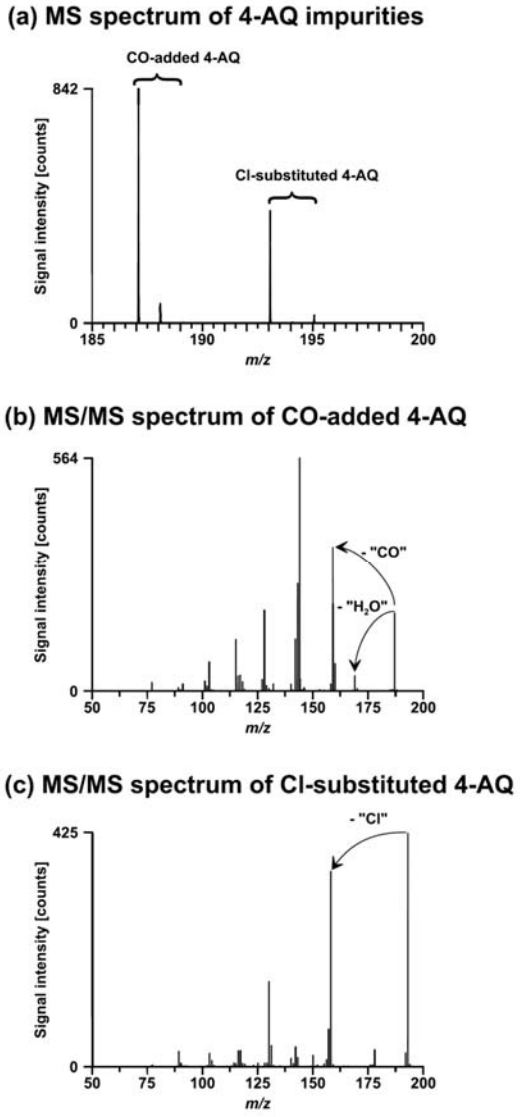

Figure S5. ESI-MS and -MS/MS spectra of impurities identified in *F*.

2.1.3 Possible Impurities

Molecular Weight (Mr) 192

- x-Chloro-2-methyl-4-quinolinamine (e.g., 68017-47-0, 66735-24-8, 68017-48-1, 58550-88-2)

Molecular Weight (Mr) 186

- 4-Amino-2-methyl-x-quinolinecarboxaldehyde (e.g., 99984-36-8, 63481-71-0)
- *N*-(2-Methyl-4-quinolinyl)-formamide (1483346-88-8)

2.2 Solvent Screening using SA Sample

The solid form screen published in ref. 8 was REPEATED using the *SA* and *F* samples as obtained from the supplier.

2.2.1 Evaporative Crystallisation

The evaporative crystallisation screen was designed from 28 pure solvents. **4-AQ** (5–10 mg compound) was dissolved in 0.5–20 mL solvent at room temperature, then filtered either into a watch glass or vial. Vials were left open or closed with perforated caps and stored at room temperature or for faster evaporation in a drying oven at 40 °C. Residues were analysed with PXRD. The results of the evaporative crystallisation screen are summarised in Table S5 and agree with the previously obtained results given in ref. 8.

Table S5. Summary of evaporative **4-AQ** crystallisation experiments (WG – watch glass, oV – open vial, pV – perforated vial).

Solvent	WG (RT)[a]	oV (RT)[a]	pV (RT)[a]	WG (40 °C)[a]	oV (40 °C)[a]	pV (40 °C)[a]
Methanol	□	–	–	–	–	–
Ethanol	□ > ○	–	–	–	–	–
1-Propanol	□ > ○	□	□	○	○	○
2-Propanol	□ > ○	□	□	○	○	○
1-Butanol	□+○	□	□	○	○+◇	○+◇
2-Butanol	□	□	□	○	○	○
1-Pentanol	□+○	□	□	○	○	○
2-Pentanol	□	□	□	○	○	○
t-Pentanol	□+○	□	□	○	○	○
Acetone	□	–	–	–	–	–
Acetonitrile	□+○	–	–	–	–	–
Dimethyl formamide	□+○	–	–	diff. cpd	–	–
Dimethyl sulfoxide	□	–	–	diff. cpd	–	–
Dichloromethane	□+○	□+○	□+○	○	○	○
Dichloroethane	□+○	□+○	□+○	○	○	○
Chloroform	○+◇	□+○	□+○	○	○	○
Carbon tetrachloride	X(S_{CCl4})	S_{CCl4}	S_{CCl4}	○+ X(S_{CCl4})	◇ S_{CCl4} [b]	◇ S_{CCl4} [b]
1,4-Dioxane	□+○	–	–	–	–	–
Methyl acetate	□+○	–	–	–	–	–
Ethyl acetate	□+○	–	–	–	–	–
Diethyl ether	□+○	–	–	–	–	–
Ethyl methyl ketone	○	–	–	–	–	–
Nitromethane	○+am	–	–	–	–	–
Pyridine	□	–	–	–	–	–
Tetrahydrofurane	□+○	□+○	□	○+◇	○+◇	○+◇
Toluene	□+○					
Xylene	○					
Water	□					

[a]□= $Hy1_A$, ○ = AH I°, ◇= AH II containing residual solvent, **X** = AH III, am = amorphous, S_{CCl4} = carbon tetrachloride solvate, diff. cpd – different compound. [b]Solution saturated at 75 °C.

2.2.2 *Cooling Crystallisation*

The cooling crystallisation screen was designed from 26 pure and seven mixed solvents. Suspensions of **4-AQ** (10–25 mg in 0.5–20 mL solvents) were heated to the boiling point of the solvent, then filtered into vials. The vials were closed and cooled to room temperature (vial wrapped in Al foil) or 8 °C (refrigerator). The solid product was analysed with PXRD (Table S6). The crystallisation results are given in Table S6 and agree with the previous results.[8]

Table S6. Summary of **4-AQ** cooling crystallisation experiments.

Solvent	RT (slow)[a]	8 °C (fast)[a]	Solvent(s)	RT (slow)[a]	8 °C (fast)[a]
Methanol	○	□	Water + methanol (1:1)	□	□
Ethanol	□	□	Water + ethanol (1:1)	□	□
1-Propanol	□	□	Water + 1-propanol (1:1)	□	□
2-Propanol	□	□	Water + 2-propanol (1:1)	□	□
1-Butanol	□	□	–	–	–
2-Butanol	□	□	–	–	–
1-Pentanol	□	□	–	–	–
2-Pentanol	□	□	–	–	–
t-Pentanol	□	□	–	–	–
Acetone	□	□	Water + acetone (1:1)	□	□
Acetonitrile	○	□+○	Water + acetonitrile (1:1)	□	□
Dichloromethane	○	□	–	–	–
Dichloroethane	○	□+○	–	–	–
Chloroform	○	□+○	–	–	–
Carbon tetrachloride	S_{CCl4}	S_{CCl4}	–	–	–
Dioxane	□+○	□+○	Water + dioxane (1:1)	□	□
Methyl acetate	□	□	–	–	–
Ethyl acetate	○	□	–	–	–
Diethyl ether	○	□	–	–	–
Ethyl methyl ketone	□+○	□+○	–	–	–
Nitromethane	○	○	–	–	–
Pyridine	□	□	–	–	–
Tetrahydrofurane	○	□+○	–	–	–
Toluene	○	□	–	–	–
Xylene	○	□	–	–	–
Water	□	□	–	–	–

[a]□= $Hy1_A$, ○ = AH I°, S_{CCl4} = carbon tetrachloride solvate. RT (slow) – vial wrapped in Al foil, 8 °C (fast) – vial stored in refrigerator.

2.2.3 Antisolvent Addition Crystallisation

The antisolvent addition crystallisation screen was designed from 32 mixed solvent systems. **4-AQ** and solvents were dispensed at room temperature in various amounts, then filtered. Antisolvent was added drop-wise until either persistent clouding was observed or the maximum antisolvent volume (three times the volume of the solvent) was dispensed. Solid products were analysed with PXRD.

The results of the antisolvent addition crystallisation screen are summarised in Table S7 and agree with the previously obtained results given in ref. 8.

Table S7. Summary of **4-AQ** antisolvent addition crystallisation experiments.

Solvent	Antisolvent	Solid Form[a]	Antisolvent	Solid Form[a]
Methanol	Toluene	○	Water	□
Ethanol	Toluene	□+○	Water	□
1-Propanol	Toluene	○	Water	□
2-Propanol	Toluene	□	Water	□
1-Butanol	Toluene	□	–	–
2-Butanol	Toluene	□	–	–
Acetone	Toluene	□	Water	□
Acetonitrile	Toluene	○	Water	□
Dimethyl formamide	Toluene	□	Water	□
Dimethyl sulfoxide	Toluene	□	Water	□
Dichloromethane	Toluene	○	–	–
Dichloroethane	Toluene	○	–	–
Chloroform	Toluene	○	–	–
Carbon tetrachloride	Toluene	○	–	–
Dioxane	Toluene	○	Water	□
Methyl acetate	Toluene	○	–	–
Ethyl acetate	Toluene	○	–	–
Diethyl ether	Toluene	○	–	–
Ethyl methyl ketone	Toluene	□+○	–	–
Nitromethane	Toluene	○	–	–
Pyridine	Toluene	□	–	–
Tetrahydrofurane	Toluene	○	Water	□

[a]□= Hy1$_A$, ○ = AH I°

2.2.4 Liquid Assisted Grinding (LAG) Experiments

15–20 mg of **4-AQ** and few drops of solvent were ground in a Retsch grinding mill MM301 for 10 minutes. The wet product was analysed with PXRD. The results are summarised in Table S8. Only **Hy1$_A$** and **AH I°** were obtained in the LAG experiments.

Table S8. Summary of **4-AQ** liquid assisted grinding experiments.

Solvent	Solid Form[a]	Solvent	Solid Form[a]
Methanol	□	Carbon tetrachloride	○
Ethanol	□+○	Dioxane	○
1-Propanol	○	Methyl acetate	○
2-Propanol	○	Ethyl acetate	○
1-Butanol	○	Diethyl ether	○
2-Butanol	○	Ethyl methyl ketone	○
1-Pentanol	○	Nitromethane	○
2-Pentanol	○	Pyridine	○
t-Pentanol	○	Tetrahydrofurane	○
Acetone	○	Toluene	○
Acetonitrile	○	Xylene	○
Dimethyl formamide	○	Heptane	○
Dimethyl sulfoxide	○	Water	□
Chloroform	○	–	–

[a]□= Hy1$_A$, ○ = AH I°

2.3 Solvent Screening using SA Sample

2.3.1 Evaporative Crystallisation

Same results as section 2.2.1.

2.3.2 *Cooling Crystallisation*

Table S9. Summary of **4-AQ** cooling crystallisation experiments. Highlighted are crystallisation experiments that produced **$Hy1_B°$**.

Solvent	RT (slow)[a]	8 °C (fast)[a]	Solvent(s)	RT (slow)[a]	8 °C (fast)[a]
Methanol	○	□	Water + methanol (1:1)	□	□
Ethanol	□	□	Water + ethanol (1:1)	□	□
1-Propanol	$Hy1_B°$ + □	$Hy1_B°$ + □	Water + 1-propanol (1:1)	□	□
2-Propanol	□	□	Water + 2-propanol (1:1)	□	□
1-Butanol	□	□	–	–	–
2-Butanol	□	□	–	–	–
1-Pentanol	□	□	–	–	–
2-Pentanol	□	□	–	–	–
t-Pentanol	□	□	–	–	–
Acetone	□	□	Water + acetone (1:1)	□	□
Acetonitrile	○	□+○ > $Hy1_B°$	Water + acetonitrile (1:1)	□	□
Dichloromethane	○	□ > $Hy1_B°$	–	–	–
Dichloroethane	○	□+○	–	–	–
Chloroform	○	□+○	–	–	–
Carbon tetrachloride	S_{CCl4}	S_{CCl4}	–	–	–
Dioxane	□+○	□+○	Water + dioxane (1:1)	□	□
Methyl acetate	$Hy1_B°$ +□	$Hy1_B°$ +□	–	–	–
Ethyl acetate	○	□	–	–	–
Diethyl ether	○	□	–	–	–
Ethyl methyl ketone	□+○	□+○	–	–	–
Nitromethane	○	○	–	–	–
Pyridine	□	□	–	–	–
Tetrahydrofurane	○	□+○	–	–	–
Toluene	○	□	–	–	–
Xylene	○	□	–	–	–
Water	□	□	–	–	–

[a]□= $Hy1_A$, ○ = AH I°, S_{CCl4} = carbon tetrachloride solvate. RT (slow) – vial wrapped in Al foil, 8 °C (fast) – vial stored in refrigerator.

2.3.3 *Antisolvent Addition Crystallisation*

Same results as section 2.2.3.

2.3.4 Liquid Assisted Grinding (LAG) Experiments

Same results as section 2.2.4.

Overall, only selected cooling crystallisation experiments resulted in a different solid forms.

2.4 Hydrothermal Crystallisation Experiments

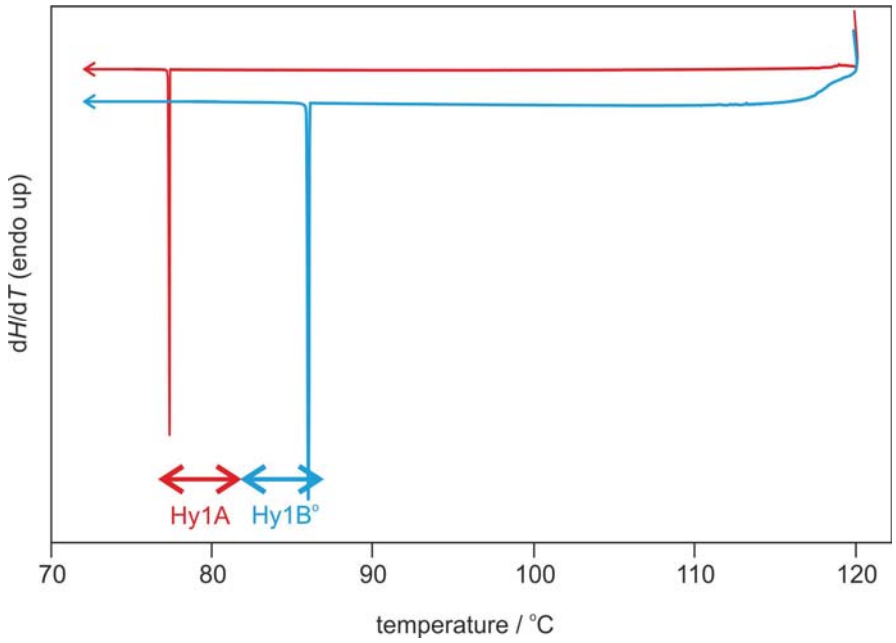

Figure S6. DSC cooling curves (0.1 K min^{-1}). Arrows mark the crystallisation ranges (temperatures) of $Hy1_A$ and $Hy1_B$°, respectively.

2.5 Water Activity Measurements

Excess 4-**AQ AH I°** was stirred (500 r.p.m.) in 1.5 – 2.5 mL of methanol:water mixtures, each containing a different mole fraction of water corresponding to a defined water activity[2,3] (Figure S7) at 25.0 ± 0.1 °C for 14 days. Samples were withdrawn, filtered and the resulting phase was determined using PXRD and TGA.

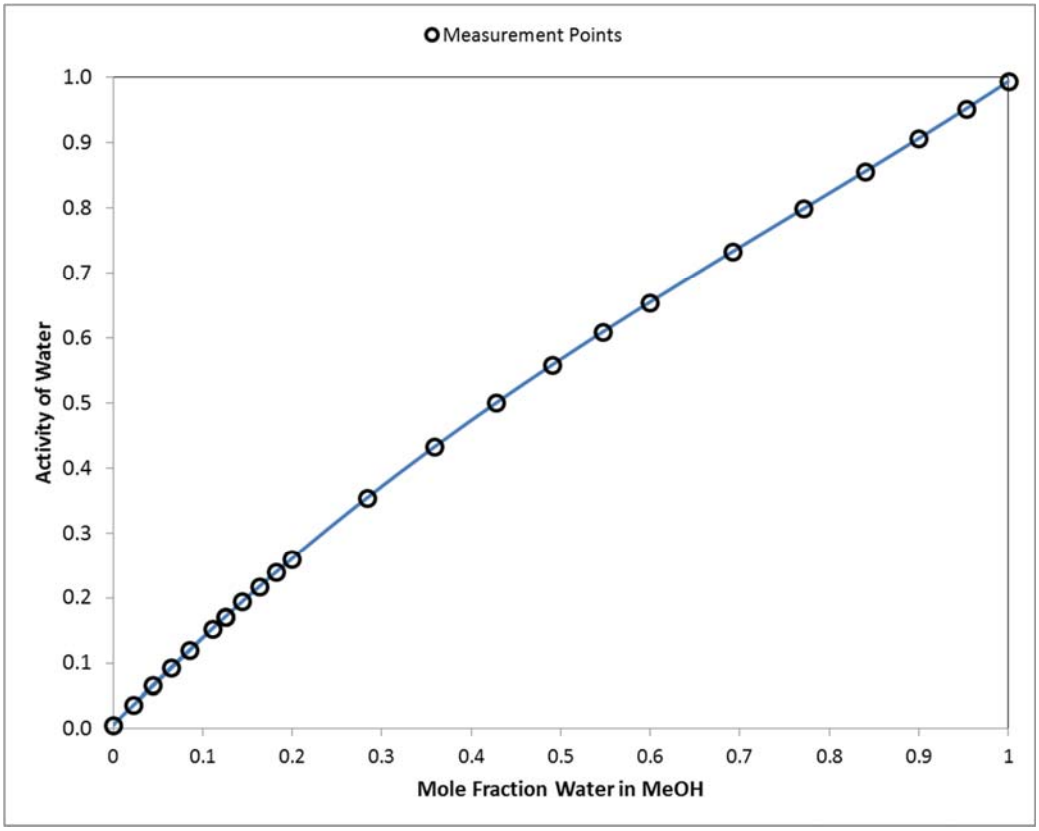

Figure S7. Plot of the water activity versus the mole fraction of water in methanol/water mixtures as 25 °C. Data from refs: 2,3.

2.6 Vibrational Spectroscopy

2.6.1 Raman Spectroscopy

Raman spectra were recorded with a Bruker RFS 100 Raman-spectrometer (Bruker Analytische Messtechnik GmbH, D), equipped with a Nd:YAG Laser (1064 nm) as the excitation source and a liquid-nitrogen-cooled, high sensitivity Ge-detector. The spectra (128 scans per spectrum) were recorded in aluminium sample holders with a laser power of 300 mW and a resolution of 4 cm^{-1}.

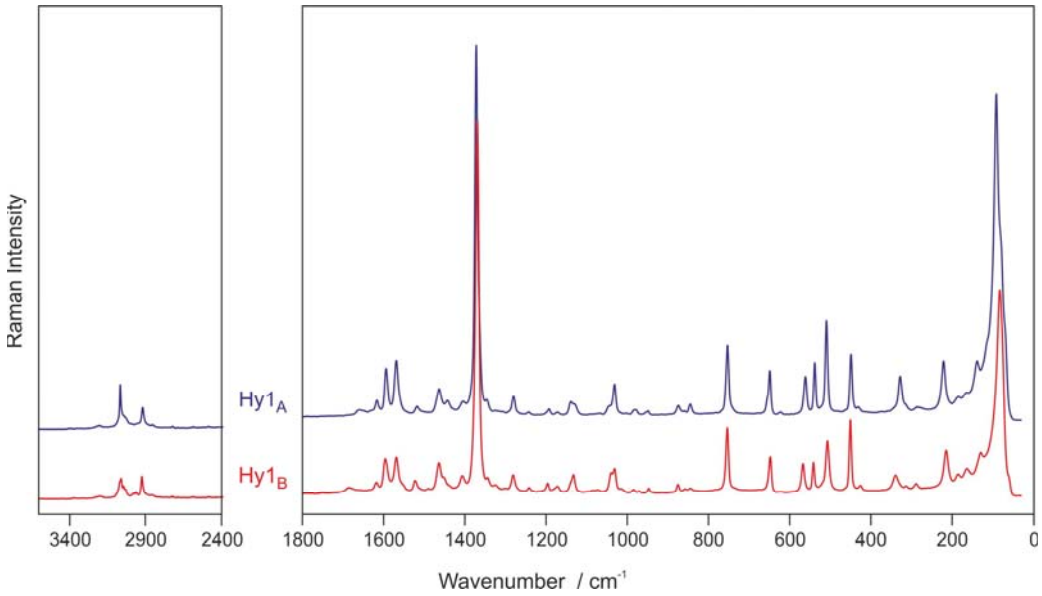

Figure S8. FT-Raman spectra of 4-**AQ** monohydrate polymorphs.

2.6.2 Infrared Spectroscopy

FT-IR spectra were recorded with a Bruker IFS 25 spectrometer connected to a Bruker IR microscope I with a 15x-Cassegrain-objective (Bruker Analytische Messtechnik GmbH, Ettlingen, Germany). The samples were prepared on ZnSe discs and following measurement conditions were applied: spectral range 4000 to 600 cm^{-1}, resolution 4 cm^{-1}, 64 scans per spectrum.

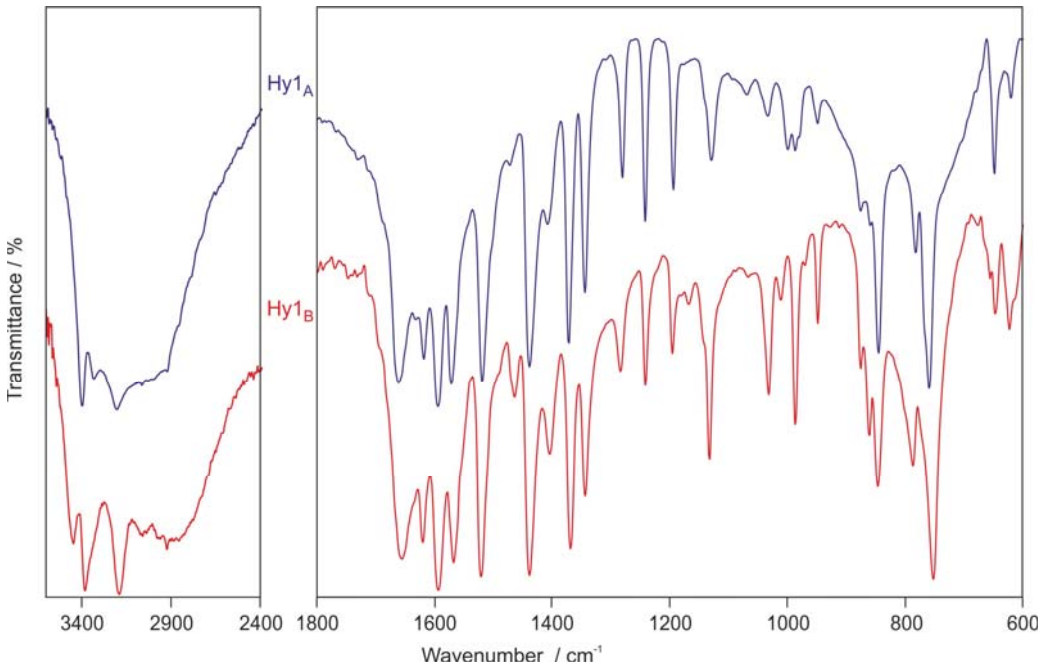

Figure S9. FT-IR spectra of **4-AQ** monohydrate polymorphs.

2.7 Structure Comparison

	Hy1$_A$ (LOBSOL)	**Hy1$_B$°**
a	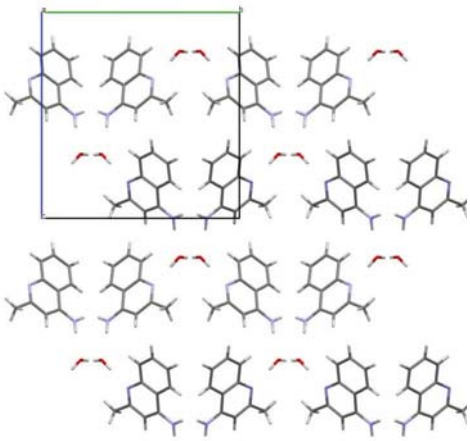	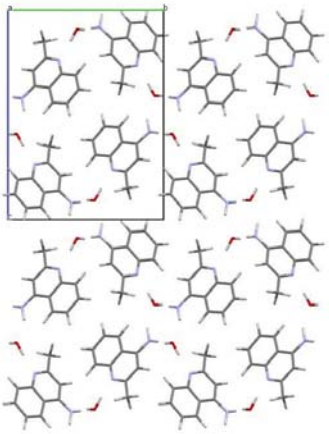
b	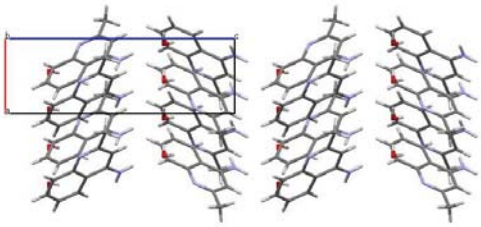	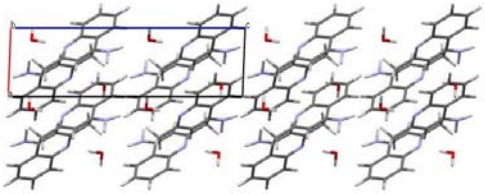
c	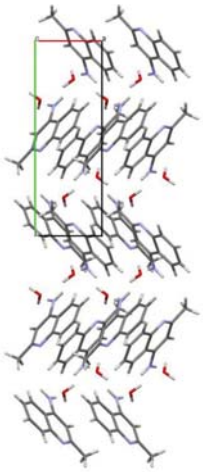	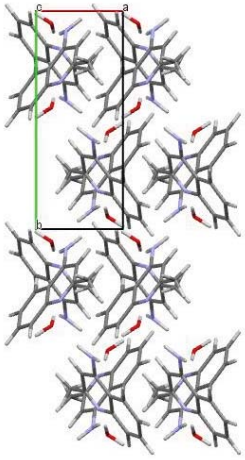

Figure S10. Packing comparison of 4-AQ monohydrate polymorphs view along crystallographic axes *a*, *b*, and *c*.

Reference List

1. Clark, S. J.; Segall, M. D.; Pickard, C. J.; Hasnip, P. J.; Probert, M. J.; Refson, K.; Payne, M. C. *Z. Kristallogr.* **2005,** *220*, 567-570.

2. Perdew, J. P.; Burke, K.; Ernzerhof, M. *Phys. Rev. Lett.* **1996,** *77*, 3865-3868.

3. Vanderbilt, D. *Phys. Rev. B* **1990,** *41*, 7892-7895.

4. Tkatchenko, A.; Scheffler, M. *Phys. Rev. Lett.* **2009,** *102*, 073005-1-073005/4.

5. Grimme, S. *J. Comput. Chem.* **2006,** *27*, 1787-1799.

6. Spek, A. L. *Acta Crystallographica Section D* **2009,** *65*, 148-155.

7. Chisholm, J. A.; Motherwell, S. *J. Appl. Crystallogr.* **2005,** *38*, 228-231.

8. Braun, D. E.; Gelbrich, T.; Kahlenberg, V.; Griesser, U. J. *CrystEngComm* **2015,** *17*, 2504-2516.